LETTER

Structural basis of CRISPR–SpyCas9 inhibition by an anti–CRISPR protein

De Dong[1]*, Minghui Guo[1]*, Sihan Wang[1]*, Yuwei Zhu[1], Shuo Wang[1], Zhi Xiong[1], Jianzheng Yang[1], Zengliang Xu[1] & Zhiwei Huang[1]

CRISPR–Cas9 systems are bacterial adaptive immune systems that defend against infection by phages. Through the RNA-guided endonuclease activity of Cas9 they degrade double-stranded DNA with a protospacer adjacent motif (PAM) and sequences complementary to the guide RNA[1–5]. Recently, two anti-CRISPR proteins (AcrIIA2 and AcrIIA4 from *Listeria monocytogenes* prophages) were identified, both of which inhibit *Streptococcus pyogenes* Cas9 (SpyCas9) and *L. monocytogenes* Cas9 activity in bacteria and human cells[6]. However, the mechanism of AcrIIA2- or AcrIIA4-mediated Cas9 inhibition remains unknown. Here we report a crystal structure of SpyCas9 in complex with a single-guide RNA (sgRNA) and AcrIIA4. Our data show that AcrIIA2 and AcrIIA4 interact with SpyCas9 in a sgRNA-dependent manner. The structure reveals that AcrIIA4 inhibits SpyCas9 activity by structurally mimicking the PAM to occupy the PAM-interacting site in the PAM-interacting domain, thereby blocking recognition of double-stranded DNA substrates by SpyCas9. AcrIIA4 further inhibits the endonuclease activity of SpyCas9 by shielding its RuvC active site. Structural comparison reveals that formation of the AcrIIA4-binding site of SpyCas9 is induced by sgRNA binding. Our study reveals the mechanism of SpyCas9 inhibition by AcrIIA4, providing a structural basis for developing 'off-switch' tools for SpyCas9 to avoid unwanted genome edits within cells and tissues.

CRISPR–Cas (clustered regularly interspaced short palindromic repeats and CRISPR-associated proteins) systems are adaptive immune systems that are encoded by about 90% of archaea and 50% of bacteria to protect against invasion by phages[1–5]. The CRISPR–Cas immunity response consists of three stages[7–9]. During the adaptation stage, also known as spacer acquisition, the processed foreign DNA (known as the protospacer) is integrated into the CRISPR array locus, yielding a new spacer. The crRNA expression and processing stage involves transcription of the CRISPR locus into a single pre-CRISPR RNA (pre-crRNA) and further processing into mature crRNAs. In the interference stage, a single Cas protein (or complex) uses the crRNA as a guide to cleave phage nucleic acid or plasmid bearing a complementary sequence to the spacer sequence of the crRNA. The CRISPR–Cas systems are classified into two classes that are divided into six types (I–VI) and nineteen subtypes on the basis of the identities of the Cas proteins.

The well-characterized *S. pyogenes* Cas9 (SpyCas9) system, which belongs to type II-A CRISPR subtype, recruits target double-stranded DNA (dsDNA) through recognition of the PAM segment by the PAM-interacting domain[10–15]. After separation of the two strands of target dsDNA, the target strand forms the heteroduplex with the guide sequence of crRNA. The complementary and non-complementary strands of DNA are cut by the nuclease domains of HNH and RuvC, respectively[14,15]. SpyCas9 combined with a synthetic single-guide RNA (sgRNA) has been harnessed as the most common and powerful tool for genome editing and gene regulation in various organisms[16–18]. However, there is still a lack of effective methods of exerting control over SpyCas9 activity, and thereby reducing the off-target genome edits caused by excessive or prolonged SpyCas9 activity[19–26]. To this end, a recent study opened the possibility of modulating the activity of the Cas9-editing system[6]. Four distinct anti-CRISPR proteins encoded by *L. monocytogenes* prophages were identified, and two of them, AcrIIA2 (the isoelectric point (pI) = 3.91, 14 kDa) and AcrIIA4 (pI = 4.11, 10 kDa) were found to inactivate the type II-A CRISPR–Cas9 proteins of *L. monocytogenes* Cas9 (LmoCas9) and SpyCas9 *in vivo*. AcrIIA4 nearly completely blocked catalytically deactivated SpyCas9-based gene repression in *Escherichia coli*, and potently prevented SpyCas9-mediated gene editing in human cells[6]. Therefore, AcrIIA2 and AcrIIA4 represent potential tools in the toolkit of Cas9-mediated genome editing; however, the molecular mechanism by which AcrIIA2 or AcrIIA4 block Cas9 activity is unknown.

To determine whether AcrIIA2 and AcrIIA4 function by directly interacting with SpyCas9, we used gel filtration to assay interaction of the purified SpyCas9 protein with AcrIIA4. Unexpectedly, AcrIIA4 protein did not display interaction with SpyCas9 under the tested conditions (Fig. 1a). However, in the presence of sgRNA, AcrIIA4 co-migrated with SpyCas9 (Fig. 1a), suggesting that they formed sgRNA-induced complexes. This conclusion is further confirmed by our glutathione *S*-transferase (GST) pull-down assay using both AcrIIA2 and AcrIIA4 proteins (Extended Data Fig. 1). In contrast, AcrIIA2 and AcrIIA4 did not associate with sgRNA-bound *N. meningitidis* Cas9 (NmeCas9)[27] (Fig. 1a, Extended Data Fig. 1), a distantly related type II-C Cas9 homologue with about 15% sequence identity to SpyCas9 (Extended Data Fig. 2). These data demonstrate that the anti-CRISPR proteins AcrIIA2 and AcrIIA4 specifically bind to SpyCas9 in its sgRNA-bound state. Owing to the difficulty in purification of LmoCas9, we were unable to test the interaction of this Cas9 protein with AcrIIA2 or AcrIIA4. However, given its conserved sequence (shares 53% sequence identity with SpyCas9, Extended Data Fig. 2) and similar activity to SpyCas9 (ref. 6), LmoCas9 probably uses a similar mechanism to recognize AcrIIA2 or AcrIIA4.

To assess the effect of AcrIIA2 and AcrIIA4 on the enzymatic activity of SpyCas9 *in vitro*, we performed DNA cleavage assays using purified proteins. Consistent with previous observations[10], SpyCas9 pre-incubated with sgRNA efficiently cleaved target dsDNA containing the 5′-TGG-3′ PAM sequence (Fig. 1b). Addition of the anti-CRISPR protein AcrIIA2 or AcrIIA4 resulted in dose-dependent suppression of SpyCas9-catalysed cleavage of the target dsDNA (Fig. 1b). This result was consistent with previous data from cell-based assays[6]. Taken together, our biochemical results demonstrate that AcrIIA2 and AcrIIA4 directly and specifically bind SpyCas9 and inhibit its dsDNA-cleavage activity.

To elucidate the molecular mechanism of SpyCas9 inhibition by anti-CRISPR AcrIIA4, we determined the crystal structure of the SpyCas9–sgRNA–AcrIIA4 complex at 3.0 Å resolution (Extended Data Table 1). In complex, SpyCas9 has a bi-lobed architecture (Fig. 2a, b), and a central channel formed between the REC and the NUC lobes as previously

---

[1]HIT Center for Life Sciences, School of Life Science and Technology, Harbin Institute of Technology, Harbin 150080, China.
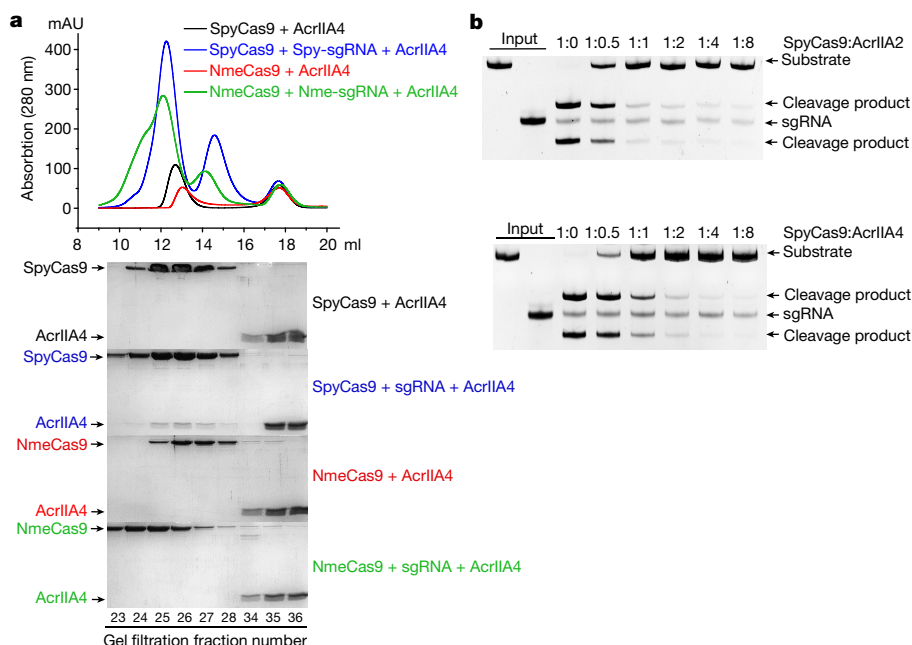*These authors contributed equally to this work.

Figure 1 | AcrIIA2 and AcrIIA4 inhibit SpyCas9 activity by directly interacting with the sgRNA-bound SpyCas9. a, Gel filtration experiments assaying the ability of AcrIIA4 to interact with SpyCas9. Top, UV absorbance (280 nm) peaks from size-exclusion chromatography of various proteins indicated. Bottom, SDS–PAGE and Coomassie blue staining of the peak fractions from gel filtration shown on the top. Colour codes are indicated. **b**, AcrIIA2 (upper panel) and AcrIIA4 (lower panel) inhibit SpyCas9 DNase activity. Molar ratios of anti-CRISPR protein/SpyCas9 are shown at the top of each lane. The reactions were stopped by adding loading buffer for denaturing gel and the reaction mixtures were run on TBE-urea polyacrylamide gels and visualized by ethidium bromide staining. Data shown are representative of three independent experiments.

observed[12–15]. AcrIIA4 binds the concave surface of SpyCas9 formed by C-terminal domain (CTD), TOPO and RuvC domains (Fig. 2a, b). The overall structure of SpyCas9 is nearly identical to that of the sgRNA-bound SpyCas9 structure[12] (Extended Data Fig. 3a), indicating that AcrIIA4 binding does not induce substantial conformational changes in the sgRNA-bound SpyCas9.

AcrIIA4 in the complex maintains a single-domain structure with highly negative charges on its surface (Fig. 3a). DALI search (http://ekhidna.biocenter.helsinki.fi/dali_server) identified no structures appreciably similar to that of AcrIIA4, indicating that the AcrIIA4 protein possesses a novel fold. AcrIIA4 comprises a three-helix bundle packing against a two-stranded anti-parallel β-sheet (Fig. 3a). AcrIIA4 is located in the region around the junction of TOPO, CTD and RuvC domains of SpyCas9 with extensive charge and surface complementarities (Fig. 3b). At the interface with TOPO, residues Asp14 and Asn36 from the α1–β1 and β1–β2 of AcrIIA4 form polar contacts with residues Glu1108, Ser1109 and Ser1136 of TOPO, respectively (Fig. 3c). Arg1333 and Arg1335 from a β-hairpin of CTD are recognized by the α1–α2 loop of AcrIIA4, forming five hydrogen bonds with Tyr67, Asp69, Glu70 and Asn39 (Fig. 3d). In addition, Asp37 and Glu40 from
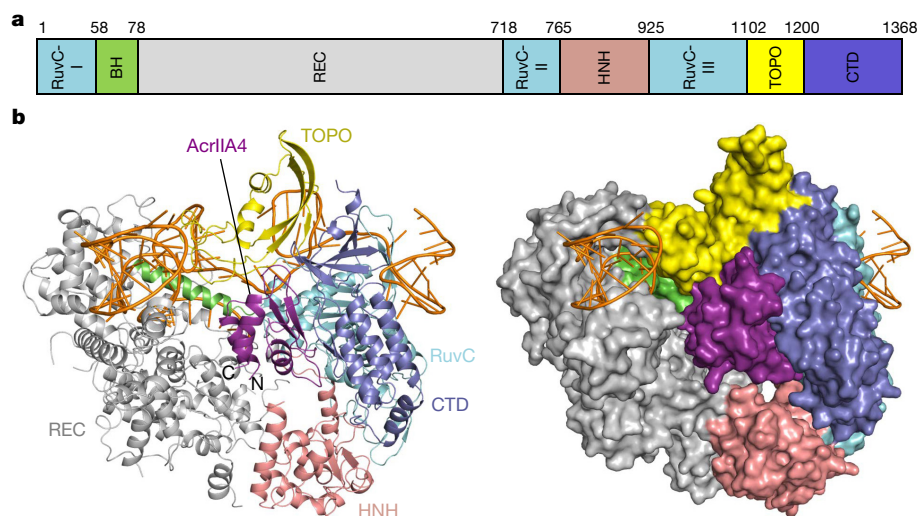

Figure 2 | Overall structure of AcrIIA4–SpyCas9–sgRNA. a, Schematic diagram of domain organization of SpyCas9. SpyCas9 protein comprises an RNA recognizing lobe (REC), a nuclease (NUC) lobe containing two nuclease domains (HNH and RuvC) and a PAM-interacting domain. The PAM-interacting domain can be further divided into a topoisomerase-homology (TOPO) domain and a C-terminal domain (CTD). BH, bridge helix. **b**, Overall structures of the AcrIIA4–SpyCas9–sgRNA complex shown in ribbon (left panel) and surface representation (right panel). Individual SpyCas9 domains are coloured according to the scheme in **a**. AcrIIA4 and sgRNA are coloured purple and orange, respectively.
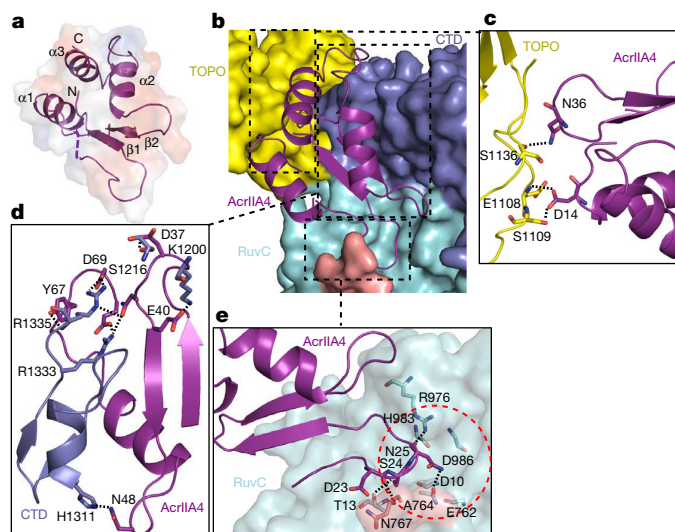
Figure 3 | Structural mechanism of AcrIIA4 recognition by SpyCas9. a, Overall structure of AcrIIA4 shown in cartoon representation and electrostatic potential surface representation. White, blue and red indicate neutral, positive and negative surfaces, respectively. **b–e**, The interfaces of AcrIIA4 (in cartoon) with TOPO, CTD and RuvC domains of SpyCas9 (in surface) (**b**). **c–e**, Detailed interactions of AcrIIA4 with TOPO (**c**), CTD (**d**) and RuvC (**e**) domains of SpyCas9. Hydrogen bonds are shown as dashed lines.

one side of the β1–β2 hairpin of AcrIIA4 hydrogen bond with Ser1216 and Lys1200, respectively, whereas Asn48 from the other side contacts His1311 to further enforce the interaction (Fig. 3d). Notably, the protruding loop preceding β1 (resides Leu19–Gln29) of AcrIIA4 completely covers the substrate entrance of the RuvC active site (residues Asp10, Glu762, His983 and Asp986) through interaction with Asn767, Thr13, Ala764 and Arg976 of RuvC by Asp23, Ser24 and Asn25 (Fig. 3e). This suggests that blocking substrate from accessing to the RuvC active site is important for AcrIIA4 to suppress the enzymatic activity of SpyCas9. Supporting this structural observation, we found

that mutation of residues around the AcrIIA4–SpyCas9 interface impaired their interaction (Extended Data Fig. 3b) and resulted in non-detectable AcrIIA4-mediated inhibition of SpyCas9 (Extended Data Fig. 3c). The AcrIIA4 mutants D23R and G38A substantially reduced binding affinity for SpyCas9 (not shown), and the reduced SpyCas9-binding activity allowed easier replacement of these two AcrIIA4 mutant proteins by a dsDNA substrate, explaining the compromised inhibition of SpyCas9 (Extended Data Fig. 3c).

Structure-based sequence alignment revealed that the AcrIIA4-interacting residues of SpyCas9, including Asn767, Arg1333, Arg1335, Ser1216 and Lys1200, are conserved in LmoCas9 (Extended Data Fig. 2) but not in NmeCas9, which suggests why AcrIIA4 was unable to interact with NmeCas9 (Extended Data Fig. 1).

Structural comparison of the SpyCas9–sgRNA–AcrIIA4 and SpyCas9–sgRNA–DNA structures revealed that the AcrIIA4-binding site on the PAM-interacting domain completely overlaps with that of the PAM DNA-binding site of SpyCas9 (Fig. 4a). Further structural analyses showed that the acidic side residues Asp14, Asp37, Glu40, Asp69 and Glu70 of AcrIIA4 are located in positions equivalent to several phosphates of the PAM double-stranded DNA backbone (Fig. 4b, c). Notably, these AcrIIA4 residues also interact with the essential PAM-interacting residues[12] Glu1108, Ser1109, Ser1216, Lys1200, Arg1335 and Arg1333 from the PAM-interacting domain of SpyCas9 (Fig. 4b, c). These structural analyses indicate that AcrIIA4 inhibits SpyCas9 through occupation of the PAM-binding site of SpyCas9, thus blocking recognition of its substrates. In support of this conclusion, binding affinity quantification assays using microscale thermophoresis showed that AcrIIA2 or AcrIIA4 had a much higher binding affinity for SpyCas9–sgRNA compared to a dsDNA substrate (Fig. 4d). This is further supported by the results of *in vitro* pull-down and electrophoretic mobility shift assays, both of which showed that AcrIIA2 or AcrIIA4 competed with a PAM-containing dsDNA substrate to bind SpyCas9–sgRNA (Extended Data Fig. 3d, e, Extended Data Table 2). Interestingly, structural alignment of AcrIIA4–SpyCas9–sgRNA and dsDNA–SpyCas9–sgRNA showed that the conformations of PAM-interacting domain and RuvC of SpyCas9 interacting with both PAM and AcrIIA4 are nearly identical. By contrast, the conformations of REC lobe and HNH domains are markedly different in the two
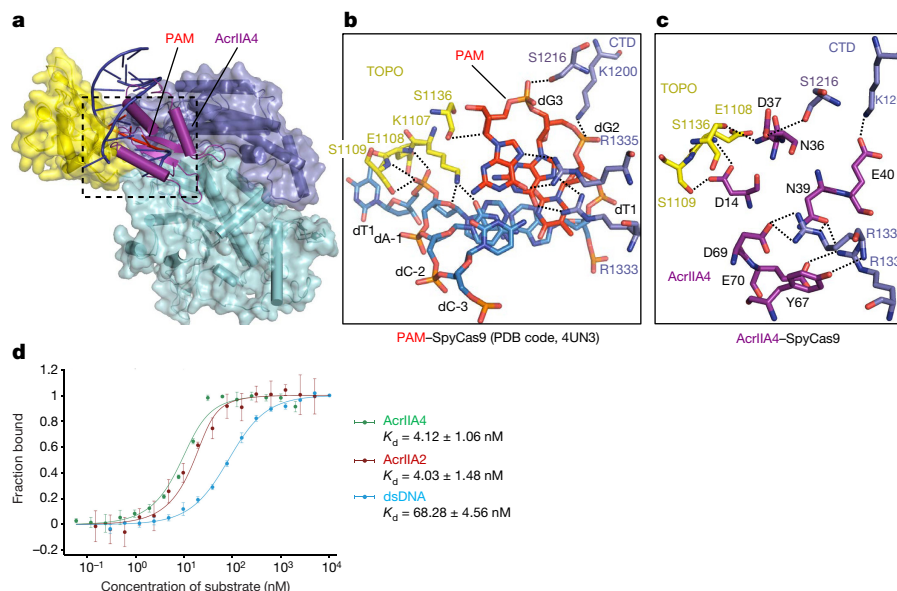

Figure 4 | AcrIIA4 and PAM sequence overlap when interacting with SpyCas9 a, Superimposition of the structures of AcrIIA4–SpyCas9–sgRNA and SpyCas9–sgRNA–dsDNA (PDB, 4UN3). AcrIIA4- and PAM- (in red) containing dsDNA are shown in cartoon representations, and SpyCas9 is shown in cartoon and transparent surface representations. **b, c**, Detailed interactions of PAM (**b**) and AcrIIA4 (**c**) with SpyCas9.

The side chains from PAM, AcrIIA4 and SpyCas9 are labelled and shown as indicated. **d**, Quantification of the binding affinity of AcrIIA2, AcrIIA4 and PAM-containing dsDNA with SpyCas9–sgRNA using microscale thermophoresis. Data shown are representative of three independent experiments. The errors were calculated as standard deviations.

structures, presumably as a result binding the other part of the target DNA (Extended Data Fig. 3a). Taken together, our data support the idea that AcrIIA4 structurally mimics the PAM of a dsDNA substrate in binding to and inhibition of SpyCas9.

The catalytic mechanism of Cas9-mediated dsDNA cleavage has been extensively studied[12–15]. These studies have provided strong evidence that sgRNA binding triggers conformational changes in Cas9, creating a binding groove for recognition of a dsDNA substrate (Extended Data Fig. 4). The sgRNA-dependent dsDNA substrate binding to Cas9 is remarkably similar to the sgRNA-dependent AcrIIA4 interaction with and inhibition of SpyCas9 (Extended Data Fig. 4), suggesting that a similar mechanism is used by SpyCas9 for its specific recognition of AcrIIA4. Supporting this hypothesis, structural comparison showed that the AcrIIA4 binding pocket of free SpyCas9 is much less well defined compared to that of sgRNA-bound SpyCas9 (Extended Data Fig. 4). Nearly all of the AcrIIA4-interacting elements in BH, TOPO and RuvC domains of the sgRNA-free SpyCas9 are incorrectly positioned (Extended Data Fig. 4). For example, in the sgRNA-free SpyCas9 structure, a loosely packed helical bundle, composed of the N-terminal helix (residues Thr58–Arg66) of BH, a helix (residues Gly736–Ile927) of RuvC and a helix (residues Thr270–Gln285) of REC domain, completely overlaps with AcrIIA4 (Extended Data Fig. 4). These structural observations not only provide an explanation for the sgRNA-dependent AcrIIA4 inhibition of SpyCas9, but also strengthen our conclusion that AcrIIA4 blocks dsDNA substrate binding for its inhibition of SpyCas9.

In summary, the biochemical and structural data presented here reveal the mechanism underlying AcrIIA4-mediated inhibition of SpyCas9. This mechanism is reminiscent of type I anti-CRISPR that functions through direct interaction with Cas proteins to prevent DNA binding[28], and AcrF2 functions as a DNA mimic[29]. It is still unknown why the sgRNA-bound SpyCas9 but not free SpyCas9 is inhibited by AcrIIA4. But one plausible explanation could be that sgRNA-free Cas9 is short-lived in the bacterial cell. The sgRNA-dependent SpyCas9 inhibition by AcrIIA4 suggests that phages start to suppress bacterial immunity after exposing themselves to bacteria. Thus it seems that there exists an evolutionary arms race between phages and their bacterial hosts, similar to that of other pathogens with their animal or plant hosts[30]. If this is the case, it will be of interest to investigate whether bacteria evolved strategies to deal with the anti-CRISPR proteins. Whether the mechanism of AcrIIA4-mediated inhibition of SpyCas9 holds true with other anti-CRISPR proteins remains unknown. Nonetheless, our study provides a structural basis for developing of tools to temporally, spatially or conditionally control the activities of the widely used SpyCas9.

Online Content Methods, along with any additional Extended Data display items and Source Data, are available in the online version of the paper; references unique to these sections appear only in the online paper.

1. Makarova, K. S. et al. An updated evolutionary classification of CRISPR–Cas systems. Nat. Rev. Microbiol. **13**, 722–736 (2015).
2. Wiedenheft, B., Sternberg, S. H. & Doudna, J. A. RNA-guided genetic silencing systems in bacteria and archaea. Nature **482**, 331–338 (2012).
3. Marraffini, L. A. CRISPR–Cas immunity in prokaryotes. Nature **526**, 55–61 (2015).
4. Westra, E. R. et al. The CRISPRs, they are a-changin': how prokaryotes generate adaptive immunity. Annu. Rev. Genet. **46**, 311–339 (2012).
5. Sorek, R., Lawrence, C. M. & Wiedenheft, B. CRISPR-mediated adaptive immune systems in bacteria and archaea. Annu. Rev. Biochem. **82**, 237–266 (2013).
6. Rauch, B. J. et al. Inhibition of CRISPR–Cas9 with bacteriophage proteins. Cell **168**, 150–158.e10 (2017).
7. Barrangou, R. & Marraffini, L. A. CRISPR–Cas systems: prokaryotes upgrade to adaptive immunity. Mol. Cell **54**, 234–244 (2014).
8. Horvath, P. & Barrangou, R. CRISPR/Cas, the immune system of bacteria and archaea. Science **327**, 167–170 (2010).
9. van der Oost, J., Jore, M. M., Westra, E. R., Lundgren, M. & Brouns, S. J. CRISPR-based adaptive and heritable immunity in prokaryotes. Trends Biochem. Sci. **34**, 401–407 (2009).
10. Jinek, M. et al. A programmable dual-RNA-guided DNA endonuclease in adaptive bacterial immunity. Science **337**, 816–821 (2012).
11. Gasiunas, G., Barrangou, R., Horvath, P. & Siksnys, V. Cas9–crRNA ribonucleoprotein complex mediates specific DNA cleavage for adaptive immunity in bacteria. Proc. Natl Acad. Sci. USA **109**, E2579–E2586 (2012).
12. Anders, C., Niewoehner, O., Duerst, A. & Jinek, M. Structural basis of PAM-dependent target DNA recognition by the Cas9 endonuclease. Nature **513**, 569–573 (2014).
13. Nishimasu, H. et al. Crystal structure of Cas9 in complex with guide RNA and target DNA. Cell **156**, 935–949 (2014).
14. Jinek, M. et al. Structures of Cas9 endonucleases reveal RNA-mediated conformational activation. Science **343**, 1247997 (2014).
15. Jiang, F., Zhou, K., Ma, L., Gressel, S. & Doudna, J. A. Structural biology. A Cas9–guide RNA complex preorganized for target DNA recognition. Science **348**, 1477–1481 (2015).
16. Jiang, W. & Marraffini, L. A. CRISPR–Cas: new tools for genetic manipulations from bacterial immunity systems. Annu. Rev. Microbiol. **69**, 209–228 (2015).
17. Sternberg, S. H. & Doudna, J. A. Expanding the biologist's toolkit with CRISPR–Cas9. Mol. Cell **58**, 568–574 (2015).
18. Hsu, P. D., Lander, E. S. & Zhang, F. Development and applications of CRISPR–Cas9 for genome engineering. Cell **157**, 1262–1278 (2014).
19. Fu, Y., Sander, J. D., Reyon, D., Cascio, V. M. & Joung, J. K. Improving CRISPR–Cas nuclease specificity using truncated guide RNAs. Nat. Biotechnol. **32**, 279–284 (2014).
20. Hsu, P. D. et al. DNA targeting specificity of RNA-guided Cas9 nucleases. Nat. Biotechnol. **31**, 827–832 (2013).
21. Pattanayak, V. et al. High-throughput profiling of off-target DNA cleavage reveals RNA-programmed Cas9 nuclease specificity. Nat. Biotechnol. **31**, 839–843 (2013).
22. Yen, S. T. et al. Somatic mosaicism and allele complexity induced by CRISPR/Cas9 RNA injections in mouse zygotes. Dev. Biol. **393**, 3–9 (2014).
23. Orthwein, A. et al. A mechanism for the suppression of homologous recombination in G1 cells. Nature **528**, 422–426 (2015).
24. Wright, A. V. et al. Rational design of a split-Cas9 enzyme complex. Proc. Natl Acad. Sci. USA **112**, 2984–2989 (2015).
25. Nihongaki, Y., Kawano, F., Nakajima, T. & Sato, M. Photoactivatable CRISPR–Cas9 for optogenetic genome editing. Nat. Biotechnol. **33**, 755–760 (2015).
26. Nuñez, J. K., Harrington, L. B. & Doudna, J. A. Chemical and biophysical modulation of Cas9 for tunable genome engineering. ACS Chem. Biol. **11**, 681–688 (2016).
27. Pawluk, A. et al. Naturally occurring off-switches for CRISPR–Cas9. Cell **167**, 1829–1838.e9 (2016).
28. Bondy-Denomy, J. et al. Multiple mechanisms for CRISPR–Cas inhibition by anti-CRISPR proteins. Nature **526**, 136–139 (2015).
29. Chowdhury, S. et al. Structure reveals mechanisms of viral suppressors that intercept a CRISPR RNA-guided surveillance complex. Cell **169**, 47–57.e11 (2017).
30. Jorgensen, I., Rayamajhi, M. & Miao, E. A. Programmed cell death as a defence against infection. Nat. Rev. Immunol. **17**, 151–164 (2017).

Author Contributions D.D., M.G. and S.W. expressed, purified, characterized and crystallized the AcrIIA4–SpyCas9–sgRNA complex with the help of S.W., Z.X., J.Y. and Z.X. D.D., M.G., Y.Z. and Z.H. carried out crystallographic studies. D.D., M.G. and Z.H. prepared the figures. D.D. and M.G. performed in vitro transcription of sgRNA, in vitro dsDNA cleavage, GST pull-down, gel filtration, microscale thermophoresis and electrophoretic mobility shift assay experiments with the help of S.W., Z.X., J.Y. and Z.X. Z.H., D.D., M.G. and S.W. wrote the paper. All authors contributed to the manuscript preparation. Z.H. designed the experiments.

METHODS

Data reporting. No statistical methods were used to predetermine sample size. The experiments were not randomized and the investigators were not blinded to allocation during experiments and outcome assessment.

Protein expression and purification. The cDNA of full-length SpyCas9, NmeCas9, AcrIIA2 and AcrIIA4 were synthesized and sub-cloned into a bacterial expression vector pGEX-6P-1 (GE Healthcare, with an N-terminal GST tag). The proteins were expressed in *E. coli* C43 (DE3) cells. Expression of the recombinant protein was induced by 0.3 mM isopropyl β-D-1-thiogalactopyranoside (IPTG) at 16 °C. After overnight induction, the cells were collected by centrifugation, SpyCas9 was resuspended in buffer A (25 mM Tris-HCl, (pH 8.0), 1 M NaCl, 3 mM DTT) supplemented with 1 mM protease-inhibitor PMSF (phenylmethanesulphonylfluoride, Sigma). The cells were subjected to lysis by sonication and cell debris was removed by centrifugation at 23,708g for 40 min at 4 °C. The lysate was first purified using glutathione sepharose 4B (GS4B) beads (GE Healthcare). The beads were washed and the bound proteins were cleaved by precision protease in buffer B (25 mM Tris-HCl (pH 8.0), 300 mM NaCl, 3 mM DTT) overnight at 4 °C to remove the GST tag. The cleaved SpyCas9 protein was eluted from GS4B resin. Further fractionated by heparin sepharose column and ion exchange chromatography via FPLC (AKTA Pure, GE Healthcare). AcrIIA2 and AcrIIA4 proteins were resuspended in buffer B, purified as described above. Further fractionated by ion exchange chromatography.

To assemble the SpyCas9–sgRNA–AcrIIA4 complex, SpyCas9 protein was incubated with sgRNA and AcrIIA4 at the molar ratio of 1:2.5:8 at room temperature for 5 min and 4 °C for 1 h supplemented with 2 mM MgCl₂. The complex was applied onto size-exclusion chromatography (HiLoad 16/600 Superdex200, GE Healthcare) with buffer C (10 mM Tris-HCl (pH 8.0), 150 mM NaCl, 3 mM DTT) to remove excess sgRNA and AcrIIA4. Purity of the protein was monitored at all stages of the purification process using SDS–PAGE (polyacrylamide gel electrophoresis) and visualized by Coomassie blue staining. sgRNA was monitored using 6% denaturing TBE-urea and visualized by ethidium bromide staining.

Crystallization, data collection, structure determination and refinement. Crystals of the SpyCas9–sgRNA–AcrIIA4 complex were generated by mixing the protein complex with an equal amount of well solution (2 μl) by the hanging-drop vapour-diffusion method. Crystals grew to their maximum size in ten days in the solution containing 0.1 M Tris-HCl (pH 6.5), 0.2 M MgCl₂ and 14% (w/v) Polyethylene glycol (PEG) 4,000 at 20 °C. Before data collection, the crystals were transferred into cryo-protectant buffer (the crystallization buffer containing 20% (w/v) glycerol) and flash-cooled in liquid nitrogen.

Diffraction data were collected at the Shanghai Synchrotron Radiation Facility (SSRF) at beam line BL19U using a DECTRIS PILATUS3 6M detector. The crystals belonged to space group *P*2₁ with one complex per asymmetric unit. The data were processed using HKL2000 (ref. 31). Molecular replacement (MR) with the program PHASER[32] was used to solve the crystal structure of the SpyCas9–sgRNA–AcrIIA4 complex. The structure of SpyCas9–sgRNA (PDB, 4ZT0) was first used as a search model for MR. The electron density calculated to 3.0 Å was sufficient for building the model of AcrIIA4 with the program COOT[33]. The complex model was refined by the program PHENIX[34]. The structural figures were prepared using PYMOL[35].

***In vitro* transcription and purification of sgRNA.** The sgRNA was transcribed *in vitro* using T7 polymerase and purified using corresponding concentration denaturing polyacrylamide gel electrophoresis. Transcription template (dsDNA) for sgRNA was generated by PCR. Buffer containing 0.1 M HEPES-K (pH 7.9), 12 mM MgCl₂, 30 mM DTT, 2 mM Spermidine, 2 mM each NTP, 80 μg ml⁻¹ home-made T7 polymerase and 500 nM transcription template was used for the transcription reactions. The reactions were processed at 37 °C for 2–6 h and stopped by 1 h at −80 °C. Pyrophosphate precipitated with Mg²⁺ at cold temperatures, and DNA templates precipitated with Spermidine. After the precipitation was removed, RNAs was precipitated by ethanol precipitation. The RNA-containing pellets were then resuspended and purified by gel electrophoresis on a denaturing (8 M Urea) polyacrylamide gel. RNA bands were excised from the gel and recovered with Elutrap System followed by ethanol precipitation. RNAs were resuspended in diethyl pyrocarbonate H₂O and stored at −80 °C.

***In vitro* cleavage assay.** *In vitro* dsDNA cleavage reactions were performed in a 20 μl buffer system containing 0.6 μg SpyCas9, 0.1 μg sgRNA and 0.3 μg dsDNA. Target DNA sequence containing a protospacer target sequence and a 5′-TGG-3′ PAM motif was cloned into pUC18 vector. To test AcrIIA-protein-mediated inhibition of dsDNA cleavage by SpyCas9, molar ratios of SpyCas9–AcrIIA ranging from 1:0 to 1:8 were used. Cleavage reactions were conducted at 37 °C for 15 min in cleavage buffer (20 mM Hepes-Na (pH 7.5), 2 mM MgCl₂, 100 mM KCl, 1 mM dithiothreitol, 5% glycerol). Reactions were stopped by adding 2× TBE-urea gel loading buffer and 95 °C quenching for 5 min. Cleavage products were run on TBE-urea 6% PAGE and visualized by ethidium bromide staining.

GST pull-down assay. Purified GST–SpyCas9 and GST–NmeCas9 were incubated with purified cognate sgRNA and AcrIIA2 or AcrIIA4 protein (molar ratio, 1:2:8) at 4 °C for 15 min. 40 μl GS4B resin was added into each reaction system and incubated at 4 °C for 10 min after washing three times with buffer B. In the interface residues disrupted pull-down assay, GST-AcrIIA4 (or mutant) protein was incubated with purified SpyCas9 (or muatnt) protein and sgRNA (molar ratio, 1:1.5:3). The reaction mixtures were monitored using SDS–PAGE (polyacrylamide gel electrophoresis) and visualized by Coomassie blue staining. The experiment was repeated three times.

Microscale thermophoresis assay. The affinity of the purified SpyCas9–sgRNA complex with AcrIIA2, AcrIIA4 and dsDNA were calculated using Monolith NT. 115 (NanoTemper Technologies GmbH, Munich, Germany). Proteins were labelled with NT-647-NHS fluorescent dye. The substrate with varying concentrations (from 0.15 nM to 5 μM) was incubated with 20 nM of labelled SpyCas9–sgRNA at room temperature for 15 min in buffer containing 25 mM Tris-HCl (pH 7.5) and 100 mM NaCl. The sample was loaded into NanoTemper hydrophilic treated capillaries. Measurements were performed at 24 °C using 40% LED power and 60% microscale thermophoresis power. All experiments were repeated three times for each measurement. Data analyses were carried out using NanoTemper analysis software.

Gel filtration assay. SpyCas9 and NmeCas9 proteins were purified as described above. For complex, protein was incubated with sgRNA and AcrIIA4 at the molar ratio of 1:2.0:8 at 4 °C for 1 h, the buffer supplemented with 2 mM MgCl₂. The samples were applied onto size-exclusion chromatography (Superdex 200 increase 10/300 GL, GE Healthcare) equilibrated with buffer C. The assays were performed with a flow rate of 0.5 ml min⁻¹ and an injection volume of 1 ml for each run. Samples taken from relevant fractions were applied to SDS–PAGE and visualized by Coomassie blue staining.

Electrophoretic mobility shift assay. Electrophoretic mobility shift assays were carried out using catalytically inactive SpyCas9 protein (D10A/H840A). Non-target DNA strand 5′-end labelling was accomplished using the 5′ oligonucleotide kit (VectorLabs) with a maleimide-IR800 probe (LI-COR Biosciences, Lincoln, NE). Target and non-target DNA strands were hybridized in a 1.5:1 molar ratio after probe labelling reaction. Reactions were performed in 20 μl buffer system containing 60 ng SpyCas9, 20 ng sgRNA and 3 ng dsDNA, molar ratios of dSpyCas9:AcrIIA ranging from 1:0 to 1:8 were used. All binding reactions were conducted at 4 °C for 30 min in the buffer containing 25 mM Tris-HCl (pH 8.0), 150 mM NaCl, 3 mM DTT and 2 mM MgCl₂. The reaction mixtures were run on 6% native polyacrylamide gels and visualized by fluorescence imaging.

Data availability. The atomic coordinates and structure factors of AcrIIA4–SpyCas9–sgRNA complex has been deposited in the Protein Data Bank under the accession code 5XBL. The datasets generated and analysed during the current study are available from the corresponding authors up on reasonable request.

31. Otwinowski, Z. M. W. Processing of X-ray diffraction data collected in oscillation mode. *Methods Enzymol*. **276**, 307–326 (1997).
32. McCoy, A. J. *et al.* Phaser crystallographic software. *J. Appl. Crystallogr.* **40**, 658–674 (2007).
33. Emsley, P. & Cowtan, K. Coot: model-building tools for molecular graphics. *Acta Crystallogr. D* **60**, 2126–2132 (2004).
34. Adams, P. D. *et al.* PHENIX: building new software for automated crystallographic structure determination. *Acta Crystallogr. D* **58**, 1948–1954 (2002).
35. DeLano, W. L. PyMOL Molecular Viewer (http://www.pymol.org) (2002).
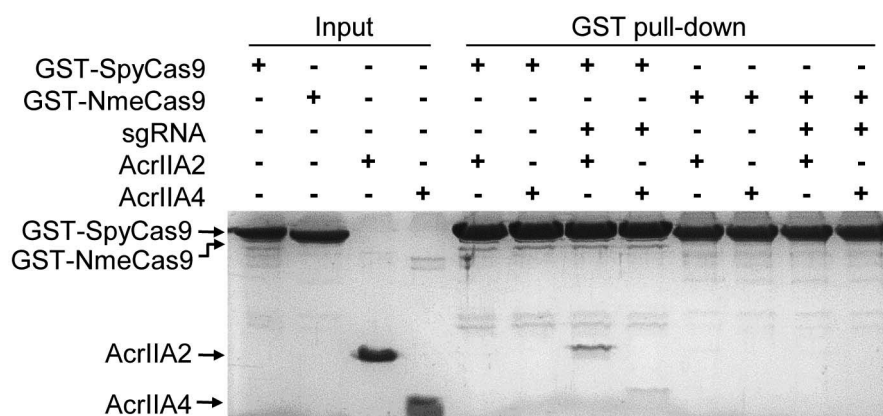
Extended Data Figure 1 | AcrIIA2 and AcrIIA4 specifically interact with sgRNA-bound SpyCas9. Binding assays were carried out between the anti-CRISPR protein of AcrIIA2 or AcrIIA4 and the GST-tagged CRISPR protein of SpyCas9 or NmeCas9 in the presence or absence of cognate sgRNA. The purified GST–SpyCas9 or GST–NmeCas9 protein was first bound to glutathione sepharose beads in the presence or absence of sgRNA, and then the beads were incubated them with AcrIIA2 or AcrIIA4 protein. After extensive washing, the bound proteins were visualized by Coomassie staining following SDS–PAGE. Data shown are the representative of three replicates.
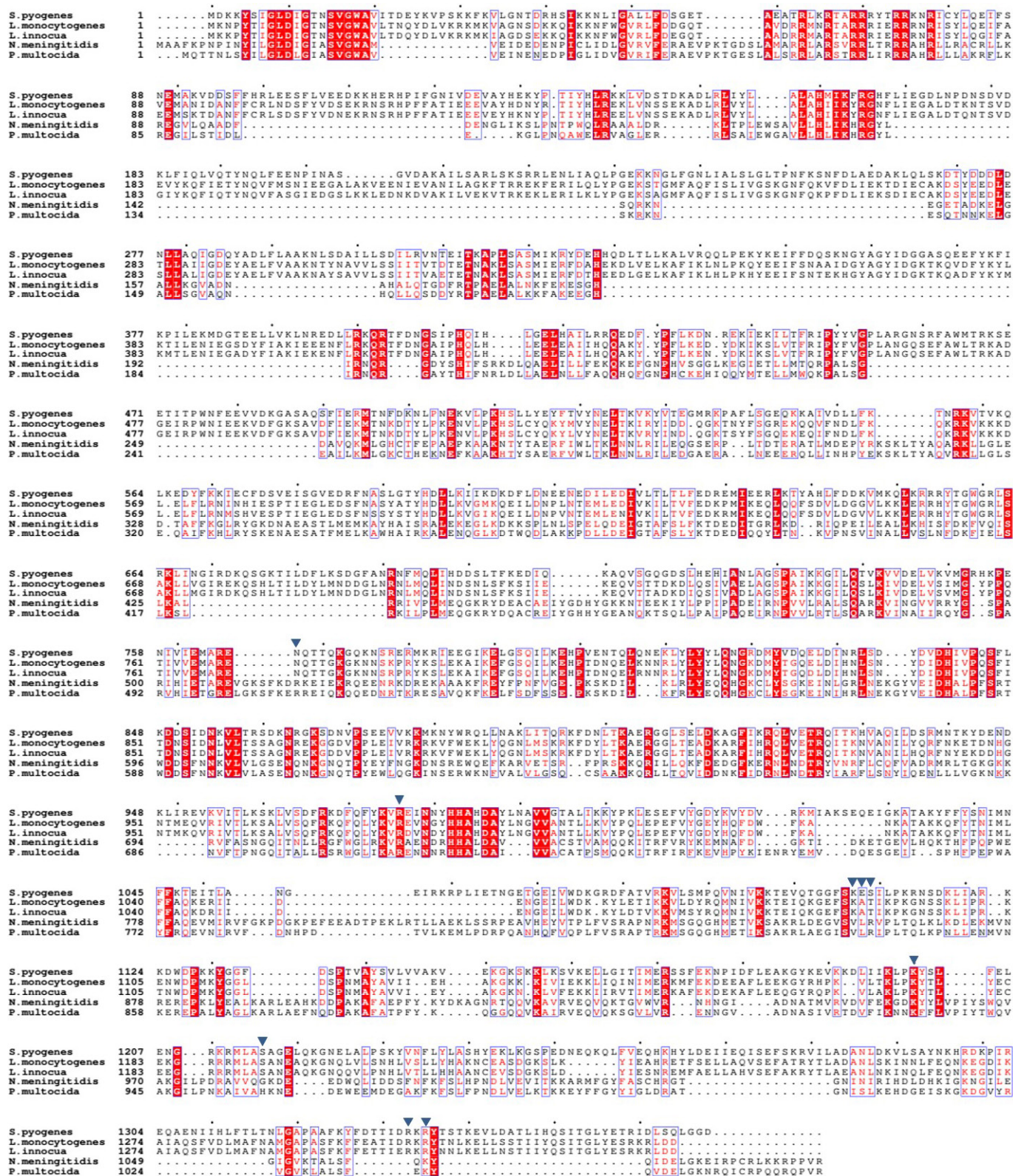
Extended Data Figure 2 | Alignment of Cas9 protein sequences.
Multiple sequence alignment of the amino acid sequences of type II-A Cas9 proteins from *Streptococcus pyogenes* (GI 15675041), *Listeria monocytogenes* J0161 (GI 345535315), *Listeria innocua* Clip11262 (GI 16414891), and type II-C Cas9 proteins of *Neisseria meningitidis* (GI 518572566), *Pasteurella multocida* subsp. *multocida* str. Pm70 (GI 218767588), aligned using MUSCLE. Residues with more than 70% similarity are shown in red and boxed in blue. Residues involved in interaction with AcrIIA4 are indicated.
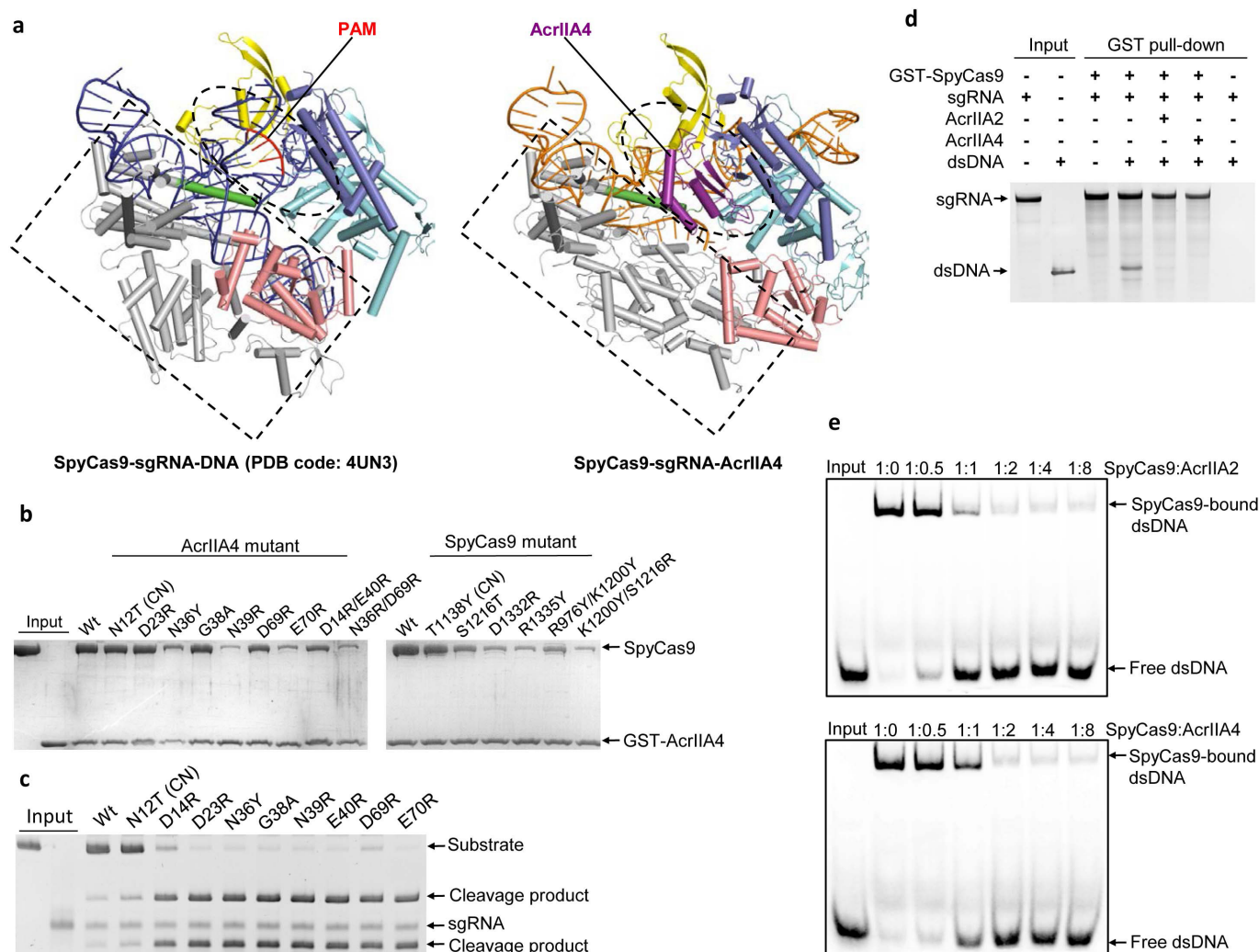
Extended Data Figure 3 | Structural comparison of SpyCas9–sgRNA–DNA and SpyCas9–sgRNA–AcrIIA4. a, Structural superimposition of SpyCas9–sgRNA–DNA (PDB code, 4UN3) and SpyCas9–sgRNA–AcrIIA4. **b,** GST pull-down assays to verify the structural determinants for preferential binding of AcrIIA4 to SpyCas9. Wild-type or mutant GST-fused AcrIIA4 proteins were first bound to glutathione sepharose beads and incubated with sgRNA-preloaded SpyCas9 (or mutant) protein as indicated. After extensive washing, the bound proteins were visualized by Coomassie staining following SDS–PAGE. **c,** Enzymatic activity assays to verify structural determinants for specific AcrIIA4–SpyCas9 interaction. The assays were performed as described in Fig. 1b. Data shown are representative of three independent experiments. **d,** AcrIIA2 and AcrIIA4 compete with PAM-containing dsDNA for binding to the SpyCas9–sgRNA. sgRNA-preloaded GST–SpyCas9 protein was first mixed with AcrIIA2 or AcrIIA4 at 4 °C and incubated for 15 min, followed by addition of PAM-containing dsDNA into the reaction mixtures. After 15 min incubation, the reactions were stopped by adding loading buffer for denaturing gel and the reaction mixtures were loaded onto glutathione sepharose beads and incubated for 15 min. After extensive washing, the bound proteins were visualized by Coomassie staining following SDS–PAGE. Data shown are representative of three independent experiments. **e,** Electrophoretic mobility shift assay results showing that AcrIIA2 and AcrIIA4 compete with PAM-containing dsDNA for binding to the SpyCas9–sgRNA. The fluorophore-labelled dsDNA and AcrIIA2 (upper panel) or AcrIIA4 (lower panel) were added to sgRNA-preloaded inactive SpyCas9(D10A/H840A) simultaneously. Molar ratios of SpyCas9–anti-CRISPR protein are shown at the top of each lane. The reaction mixtures were run on 6% native polyacrylamide gels and visualized by fluorescence imaging (800 nm). Data shown are representative of three independent experiments.
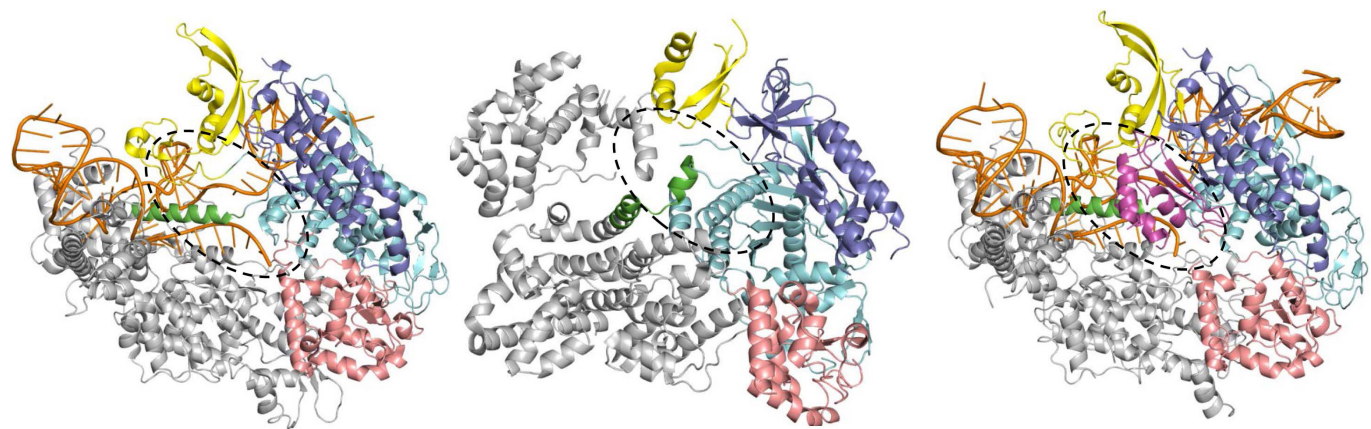
SpyCas9-sgRNA (PDB code: 4ZT0) **SpyCas9 (PDB code: 4CMP)** **SpyCas9-sgRNA-AcrIIA4**

Extended Data Figure 4 | Structural comparison of SpyCas9–sgRNA and SpyCas9. Structural superimposition of SpyCas9–sgRNA (PDB code, 4ZT0) and SpyCas9 (PDB code, 4CMP). The interface of AcrIIA4 and SpyCas9 is circled in black dashed line.

Extended Data Table 1 | Data collection, phasing and refinement statistics

	SpyCas9-sgRNA-AcrIIA4
Data collection	
Beam Line	BL19U, SSRF
Space Group	$P2_1$
Unit Cell Parameters	
a, b, c (Å)	108.41, 69.76, 129.24
α, β, γ (°)	90.0, 105.7, 90.0
Wavelength(Å)	0.9790
Resolution limits(Å)	50.00-3.05(3.10-3.05)
No. of unique reflections	33,803(1,635)
Completeness (%)	96.8(95.4)
Redundancy	3.2(2.9)
R_{merge} (%)	9.5(65.0)
Mean I/σ(I)	10.6(1.4)
Refinement	
Resolution limits(Å)	50.00-3.05
No. reflections	30160
R_{work}(%) /R_{free}(%)	23.7/27.7
R.m.s.d for bonds (Å)	0.002
R.m.s.d for angles (°)	0.677
Averaged B factor of the structure	59.7
No. of non-hydrogen protein atoms	12990
Ramachandran plot (%)	
Preferred region	90.21
Allowed region	9.79
Outliers	0.00

Highest-resolution shell is shown in parenthesis.

Extended Data Table 2 | Nucleic acid sequences used in the study

RNA sequence	Sequence (5' to 3')
SpyCas9_sgRNA	GGAAAUUAGGUGCGCUUGGCGUUUUAGAGCUAGAAAUAG CAAGUUAAAAUAAGGCUAGUCCGUUAUCAACUUGAAAAAG UGGCACCGAGUCGGUGCUU
NmeCas9_sgRNA	GGGUGCGCGGCGCAUUACCUUUACGUUGUAGCUCCCUUUC UCAUUUCGGAAACGAAAUGAGAACCGUUGCUACAAUAAGG CCGUCUGAAAAGAUGUGCCGCAACGCUCUGCCCCUUAAAG CUU
dsDNA substrate sequence	
SpyCas9_tarDNA	CAATCCCAGCCAAGCGCACCTAATTTCC
SpyCas9_tarDNA_PAM	GGAAATTAGGTGCGCTTGGCTGGGATTG
RNA transcription assay DNA temple	
SpyCas9_sgRNA_DNA templet	ATGTAATACGACTCACTATAGGAAATTAGGTGCGCTTGGCGT TTTAGAGCTAGAAATAGCAAGTTAAAATAAGGCTAGTCCGT TATCAACTTGAAAAAGTGGCACCGAGTCGGTGCTT
NmeCas9_sgRNA_DNA templet	ATGTAATACGACTCACTATAGGGTGCGCGGCGCATTACCTTT ACGTTGTAGCTCCCTTTCTCATTTCGGAAACGAAATGAGAAC CGTTGCTACAATAAGGCCGTCTGAAAAGATGTGCCGCAACG CTCTGCCCCTTAAAGCTT
DNA cleavage assay primer	
tar_BamH1_5	GATCCCAATCCCAGCCAAGCGCACCTAATTTCCG
tar_EcoR1_3	AATTCGGAAATTAGGTGCGCTTGGCTGGGATTGG
pUC18_5	TCGGTGCGGGCCTCTTCGCTATTA
pUC18_3	TTTATGCTTCCGGCTCGTATGTTG
Cleavage assay DNA sequence	
pUC18_ substrate	TCGGTGCGGGCCTCTTCGCTATTACGCCAGCTGGCGAAAG GGGGATGTGCTGCAAGGCGATTAAGTTGGGTAACGCCAG GGTTTTCCCAGTCACGACGTTGTAAAACGACGGCCAGTG CCAAGCTTGCATGCCTGCAGGTCGACTCTAGAGGATCCC AATCCCAGCCAAGCGCACCTAATTTCCGAATTCGTAATCA TGGTCATAGCTGTTTCCTGTGTGAAATTGTTATCCGCTCA CAATTCCACACAACATACGAGCCGGAAGCATAAA